Section C. Project Description

1. Introduction

The Near-Infrared Camera and Fabry-Perot Spectrometer (NIC-FPS) is an instrument being constructed at the Center for Astrophysics and Space Astronomy (CASA) at the University of Colorado – Boulder to be used on the Astrophysical Research Consortium (ARC) 3.5-m telescope at Apache Point Observatory (APO) in Sunspot, New Mexico. NIC-FPS will become the new workhorse near-IR (0.9–2.5 μm) imager for the 3.5-m telescope, replacing the GRIM II instrument. It features a fully cryogenic opto-mechanical design with a $4.6' \times 4.6'$ field of view (FOV) imaged onto a new-generation, low-noise Rockwell Hawaii-1RG 1024×1024 detector.

NIC-FPS development is funded primarily through internal resources of CU's Department of Astrophysical and Planetary Sciences (APS) – namely, from private fund-raising, Chair's discretionary funds, etc. In-kind contributions from CASA and Ball Aerospace & Technologies Corporation of Boulder are also being made to support the instrument design and construction. ARC is contributing ~$100K towards the Hawaii-1RG detector purchase, and Rice University is providing the Fabry-Perot etalon. Hence, the funding sought in this proposal is highly leveraged against the ~$1.1M invested in the instrument by CU, Rice, Ball, and ARC. NIC-FPS completed its Critical Design Review (CDR) on 26 July 2002, and major procurements (such as the Hawaii-1RG detector and optics) have begun. Instrument assembly and test will proceed through calendar year 2003, with delivery to APO scheduled for the first-quarter of 2004 and commencement of science operations by mid-2004.

Aside from being among the first near-IR instruments to employ a new, low-noise Hawaii-1RG detector, the novel aspect of NIC-FPS is the "FPS" part. Our Queensgate Instruments (QI, now IC Optical Systems) Fabry-Perot etalon provides R~10,000 (i.e., 0.01% bandpass) full-field imaging. It is one of only five *cryogenic* devices built by QI in the mid-1990's and is the *only* near-IR cryogenic tunable etalon that operates at this high spectral resolution. The very narrow bandpass of the etalon will suppress the sky background by factors of 100 to several hundred, depending on wavelength, compared to conventional near-IR 1% narrow-band imaging systems. The combination of ultra-narrow bandpass and low-noise detector will allow NIC-FPS to achieve high signal-to-noise imaging and, for some targets, full-field *kinematic mapping* in important near-IR diagnostic lines such as [Fe II]1.64μm, H_2 1-0 S(1) 2.12μm, and Br γ 2.16μm. The crux of this proposal is to secure funding to purchase narrow-band filters centered on various diagnostic near-IR features to provide order sorting for the Fabry-Perot etalon. Isolating single orders is essential to enable the full potential of this unique capability, which will achieve dramatic results in a number of scientific investigations such as probing structure and kinematics in protostellar jets, planetary nebulae (PNe), supernova remnants (SNRs), the Galactic Center, and extended emission-line regions in active galaxies. The performance will presage the potential of low-background, wide-field imaging of future ground-based (e.g., the Gemini-South Multi-Conjugate Adaptive Optics imager) and space-based (e.g., the Next Generation Space Telescope Near-Infrared Camera which features cryogenic tunable Fabry-Perot etalons) near-IR instrumentation.

2. Science Program

The Fabry-Perot etalon in NIC-FPS can be inserted into or removed from the optical beam *via* a cryogenic linear-actuator mechanism. With the etalon removed, NIC-FPS operates as a conventional near-IR imager. Three filter wheels provide slots for 17 broad-band and narrow-band science filters. The image scale of 0.27" pixel^{-1} is optimized for three-pixel sampling of the median seeing at the ARC 3.5-m telescope, and two-pixel sampling of good seeing conditions. The large-format, low-noise detector will allow the NIC-FPS direct imaging mode to far exceed the capabilities of the existing near-IR imager at ARC, both in terms of field of view and sensitivity. This in turn enables a wide array of Galactic and extragalactic science programs to be undertaken, such as follow-up near-IR imaging of high-redshift objects in Sloan Digital Sky Survey (SDSS) fields.

In this proposal, we emphasize the added *unique* capabilities enabled by the cryogenic Fabry-Perot etalon for probing the morphologies, physical conditions, and kinematics in line-emitting objects such as protostellar jets, PNe, and active galactic nuclei (AGN). The core science team on our proposed projects includes the senior personnel on this proposal (Morse, Bally, and Hartigan) who are responsible for the hardware implementation, plus Bruce Balick (University of Washington) and Stephan McCandliss (Johns Hopkins University) who reside at other ARC institutions, and Gerald Cecil (University of North Carolina). Of course, once the instrument is commissioned, we expect very broad interest from the ARC community in both the direct imaging and Fabry-Perot modes.

2.1 Stellar Outflows

We will explore mass loss in pre- and post-main sequence stars to study the origin of these outflows and their effects on the interstellar medium (ISM). Comparing observations of atomic to molecular emission-line structures will allow us to distinguish between J-shock, C-shock, magnetic precursor, reformation, and fluorescence models for the molecular emission. Line-ratio and kinematic maps will clarify how shock waves in these supersonic flows transfer momentum and energy to their environments. These diagnostics supply information about the physical conditions and time history of collimated outflows from which realistic models can be constructed.

We have performed Fabry-Perot (F-P) investigations of protostellar outflows and Herbig-Haro objects on the 4-m telescopes at CTIO and KPNO using the Rutgers R~10,000 etalon in optical emission lines (e.g., Morse et al. 1994; Hartigan et al. 2000a). These studies have yielded valuable information about the wind dynamics, shock parameters, and physical conditions in the atomic gas, but do not explore the relationship to the surrounding molecular gas. Furthermore, observing atomic and molecular lines in the near-IR will allow us to penetrate high-extinction regions near dust-enshrouded objects. We show an example of the penetrating power of near-IR observations in Figure C-1 for the case of the HH 1 jet in Orion (Reipurth et al. 2000). Other researchers have begun using Fabry-Perot etalons in the near-IR to suppress sky background (e.g., Davis et al. 2002), but no other system works both at cryogenic temperatures and with this high spectral resolution.

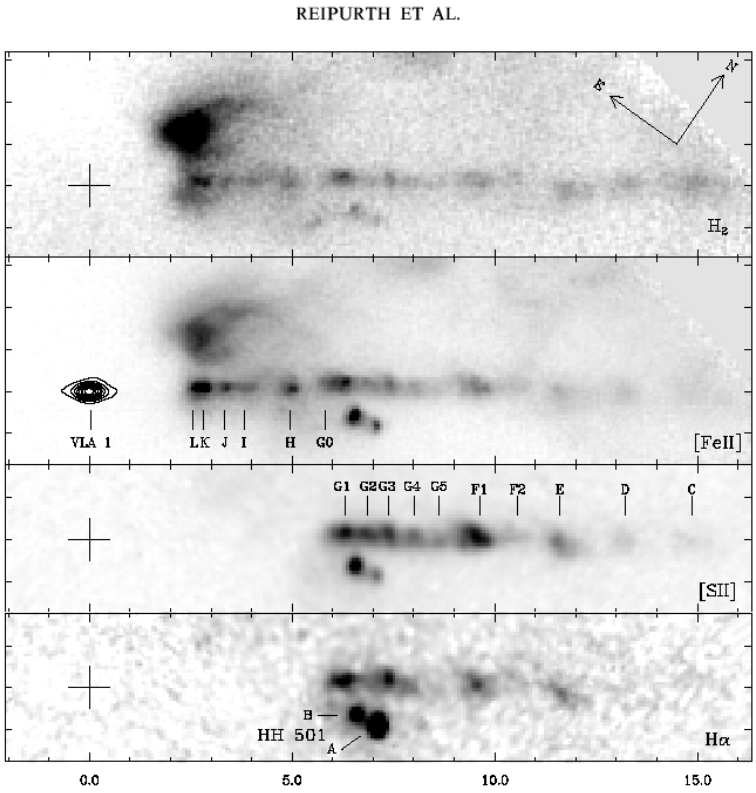

Figure C-1: *The HH 1 jet imaged by Reipurth et al. (2000) in emission from H_2 2.12μm, [Fe II] 1.64 μm, [S II] 6716,6731Å, and Hα 6563Å. Tick marks on the axes are at 1″ intervals, corresponding to ~470 pc at the distance of Orion. The near-IR emission lines allow us to trace jet shocks ~2000 AU closer to the star than the optical lines. Similar advantages will be realized for the central objects of proto-planetary nebulae and active galaxy cores.*

2.1.1 Protostellar Jets and Molecular Outflows

An extended period of mass outflow accompanies the formation of both high- and low-mass stars in our Galaxy. At large distances, molecular emission-line maps of CO taken with radio telescopes often trace poorly collimated flows that move at ~10 km s^{-1} from the young star. Closer to the star, particularly for lower mass objects, outflows can appear as highly collimated supersonic jets of material that radiate emission lines as the jet gas cools along shock fronts in the flow (Figure C-1). These stellar jets have proper motions and radial velocities that are typically hundreds of km s^{-1} with respect to the star.

The means by which outflows are driven is controversial, but there is considerable observational evidence that accretion from opaque disks onto the protostar provides the ultimate energy source for the outflows (e.g., Hartigan, Edwards, & Ghandour 1995). Outflows from young stars play a crucial role in regulating star formation, both locally by blowing away material that would otherwise accrete onto the disk and protostar, and globally by energizing molecular clouds – effectively increasing the Jean's mass required for collapse – and altering the cloud chemistry *via* processing through shock waves. Molecular clouds are probably frothy structures, permeated by bubbles driven from newly formed stars.

Stellar jets often carry enough momentum and energy to drive molecular outflows (e.g., Chernin & Masson 1995; Hartigan et al. 2000b). However, it has been difficult to quantify how a highly collimated supersonic stellar jet transfers momentum and energy to the slower, more poorly-collimated molecular flows. The jet may push molecular material ahead of it by accelerating the molecular gas directly in shock waves ("prompt" entrainment), or could drag surrounding material along the edges of the stellar jet in the wake of bow shocks in the jet ("steady" entrainment). Figure C-2 illustrates several scenarios whereby shock waves in jets may excite molecular emission as energy and momentum are transferred to the surroundings. Observations of radiative bow shocks in stellar jets suggest ballistic flow with high proper motions, which favors prompt entrainment (e.g., Hartigan et al. 2001; Reipurth et al. 2002; Bally et al. 2002), but the youngest outflows often have no optical counterparts and the molecular flow appears turbulent, as in a steady entrainment scenario (e.g., see Richer et al. 2000).

The advent of near-IR detector arrays has allowed H_2 images of star formation regions to be used to study the interface between the stellar jet and the molecular outflow (e.g., Eislöffel et al. 1994). Near-IR lines such as the 2.12 μm S(1) line of H_2 provide a crucial link between the optically visible Herbig-Haro jets and the lower-velocity molecular outflows because they radiate at intermediate temperatures between the optical and radio lines. H_2 emission probes shock velocities ranging from ~20-40 km s^{-1} in purely hydrodynamic J-shocks to >100 km s^{-1} in magnetized C-shocks, where strong magnetic fields cushion the shock and enable H_2 molecules to survive higher velocities that would otherwise dissociate molecules (Hollenbach 1997).

The goal of this aspect of our future research is to identify the physical process that best describes how collimated jets transfer momentum and energy to their surroundings, and thereby determine how bubbles are driven into the ISM by winds from young stars. Figure C-2 shows the expected spatial relationship between H_2 and optical emission lines for the different shock fronts that may excite both atomic and molecular lines. There are clear differences in the spatial location of the atomic lines (shaded areas) and H_2 emission (X's) depending on whether or not the shock has a discontinuity (J-shock), is smoothed out by a magnetic field (C-shock), or represents an intermediate case (precursor). Unique signatures of H_2 and atomic emission are also present if the H_2 reforms on grains in the dense region between the bow shock and Mach disk, or if fluorescence is important. Accompanying these spatial relationships are distinct velocity signatures; higher velocities will accompany excitation in post-shock (accelerated) regions, while lower or ambient velocities will reflect pre-shock or photon excitation.

There are numerous targets available to study in nearby star formation regions such as Taurus, Perseus, Cepheus, and Orion. Our observations will improve upon the signal-to-noise ratios obtained in exploratory narrow-band imaging programs (e.g., Stanke, McCaughrean, & Zinnecker 2000; Hartigan et al. 2000c) and will yield full-field kinematic mapping at ~30 km s^{-1} velocity resolution for tracing the transition region between the atomic and molecular flows.

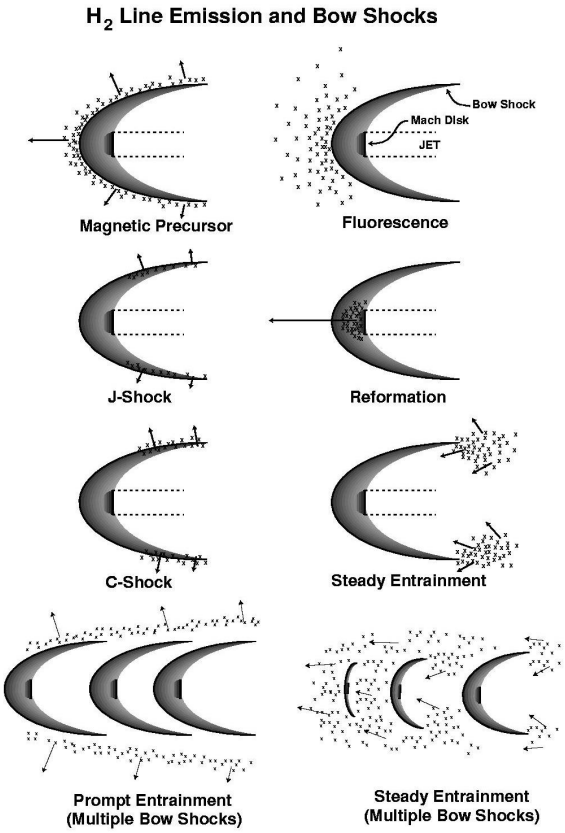

Figure C-2: *The relationship of H_2 emission (X's) to bow shocks in stellar jets expected for various models. The shaded areas show atomic line emission that arises in the cooling gas behind J-shocks in the bow shock and the Mach disk. Arrows denote the velocity of the H_2 with respect to the ambient medium. The jet flows from right to left between the dotted lines in each example. (From Hartigan et al. 1996.)*

2.1.2 Post-Main Sequence Mass Ejection

At the other end of the H-R diagram from protostellar objects are planetary nebulae, Luminous Blue Variables (LBVs, such as η Car), symbiotic stars, novae, and supernovae. Morphological studies show that these classes of stellar outflows share many, if not most, morphological characteristics and may share much of the same physics of mass ejection and collimation (e.g., Dwarkadas & Balick 1998). The value of IR observations is not to be underestimated: many of these outflows reside in dust-forming stages (proto-PNe, LBVs, novae, and symbiotics) with modest internal extinction likely, and severe extinction in some cases. Moreover, the outflowing material may be rich in molecular material affected by photodissociation regions when the central star or a companion supplies >11 eV photons and shocks where grains are sputtered and molecules and atoms are ionized. Understanding the geometric and physical relationship between molecular and atomic regions and the shocks that are likely to exist at their interfaces is a high priority for comparing to outflow models of these objects, just as it is for protostellar outflows.

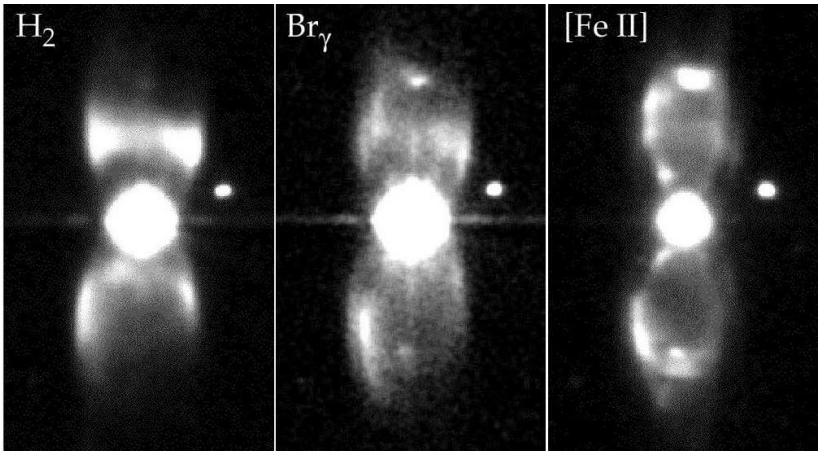

Figure C-3: *Infrared emission-line images of the M2-9 bipolar nebula (from Latter, priv. comm.) obtained at the UKIRT. Images in H_2 2.12 μm, Br γ 2.16 μm, and [Fe II] 1.64μm probe different physical conditions that identify the locations of shocks and photodissociation regions. Tracking the time evolution of the emission structures also helps to determine the nature of the central source.*

One example is illustrated in Figure C-3 from early ground-based UKIRT observations (the data are unpublished results supplied by Bill Latter). The target is M2-9, Minkowski's "Butterfly" nebula. M2-9 is classified as a planetary nebulae; however, it is likely to be associated with a symbiotic binary with a 120-yr period. Note the complementarity of all three IR images. The H_2 2.12μm image aligns well with an optical [O I] 6300,6364Å image and probably represents a photodissociation boundary at the outer edge of the mass outflow where soft UV stellar photons penetrate and excite the innermost layer of H_2. The [Fe II] 1.64μm image delineates a standing slow shock where outflowing material in the innermost lobe thermalizes before moving onward. The Brackett γ 2.16μm image is similar to the Hα optical image; however, the latter fails to show the enhanced emission along the west edge of the inner lobe which is plainly visible in the former. (Given that extinction is known to be low in the lobes, this result is puzzling indeed.)

Very little work has been done in imaging stellar outflows in highly evolved stars in the infrared. Such observations allow us to understand the hydrodynamics (perhaps the magnetohydrodynamics) of the outflows and the geometrical aspects of outflow collimation processes. All of this can be done with an efficient imaging mode. High-dispersion, low-background F-P imaging will map the patterns in the outflows – this information, coupled with imaging and proper-motion studies, provides five of the six phase-space coordinates of the nebula. When combined with density information we can measure (either from the near-IR [Fe II] 1.60/1.64 μm line ratios or Br γ flux measurements), the data allow almost direct comparison to most of the state variables calculated by HD (and MHD) models for momentum-dominated flows. Each emission line samples a complementary spatial regime (molecular, atomic, and ionized), which provides insight into the working interfaces between each zone.

2.2 Extended Emission-Line Regions in Active Galaxies

The ionized gas comprising the extended emission-line regions of active galaxies is generally presumed to represent ambient interstellar gas excited by the active nucleus. In late-type

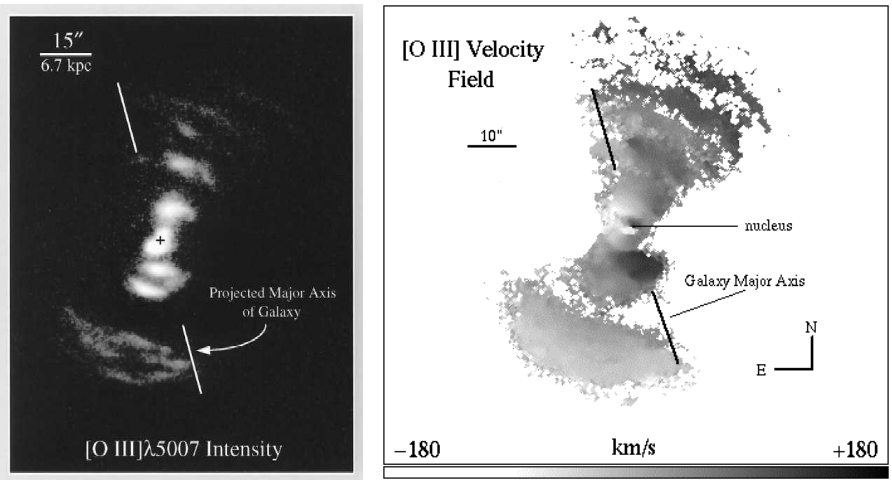

Figure C-4: *The Seyfert 2 galaxy NGC 5252 is commonly called the "poster child" for the ionization cone phenomenon. Left is a continuum-subtracted [O III]5007Å intensity image from summing individual F-P velocity slices, and right is the velocity map showing point symmetry about the nucleus. The gaseous component can be modeled as two disks oriented at different viewing angles. NGC 5252 is probably the product of a merger with a gas-rich companion galaxy. (From Morse et al. 1998.)*

galaxies, the ISM is intrinsic to the galaxy disk, while in early-type galaxies (E and S0) it may have an external origin, such as a merger with a gas-rich galaxy. An active galactic nucleus (AGN) ionizes and excites this gas; the resulting emission lines can be studied with high spatial resolution, providing a wealth of information on the physical properties, chemical abundances, kinematics, and the nature of the excitation. Close to the AGN, the kinematics are affected by the nuclear activity, but further away pure gravitational forces should dominate the motions. Thus, studies of large, extended emission-line regions can probe the settling of gas acquired by an early-type galaxy in a merger, and the relevance of such mergers for initiating nuclear activity. Furthermore, the line ratios and kinematics provide keys to the issue of whether the line emission is excited through photoionization by the active nucleus or through high-velocity shocks generated at the interface between an outflow (e.g., a radio jet) and the ISM. In the former case, the properties of the nebulosity can indicate any anisotropy in the ionizing radiation escaping from the nucleus.

Optical F-P spectrophotometric studies of nearby active galaxies have provided unique insights into the AGN phenomenon and the profound impacts they have on a galaxy's ISM (e.g., NGC 1068, Cecil et al. 1990; NGC 3079, Veilleux et al. 1995; NGC 5252, Morse et al. 1998). In the near-IR, we can extend these studies to obscured regions near the AGN and to interactions with the molecular component of the ISM. Figure C-4 shows an example of the deep imaging and full-field kinematic mapping of the extended emission-line regions of active galaxies that is possible with an R~10,000 Fabry-Perot etalon.

2.3 Filter List, Performance, and Observing Plan

The majority of funds requested in this proposal are for purchasing narrow-band filters to act as order-sorting filters for the F-P etalon. Of course, these filters can also be used in direct imaging mode. The filters will be 65 mm in diameter, which results from the beam size necessary to create the proper image scale at the detector (see Sec. 3 below). Though large, this size filter is

now becoming common for wide-field near-IR imagers (e.g., CTIO-ISPI), and allows for possible future exchanges (especially for access to southern hemisphere observatories).

Before discussing the narrow-band filters, we briefly describe the broad-band set that will be procured through internal funding. We will use the broad-band "Mauna Kea Filter Set" J, H, and K_s filters that have been ordered from Barr Associates as part of the Gemini filter consortium. The central wavelengths are 1.250, 1.635, and 2.125 μm, respectively. Participating in this large-volume procurement has resulted in substantial cost savings. Employing this standard filter set will greatly ease photometric calibration by allowing ready use of the existing standard star lists established by UKIRT and other observatories. The 65mm diameter H and K_s filters have been delivered and meet spec for high transmission (>97%) and excellent out-of-band rejection. A Z filter is also planned that matches (as well as possible) the Sloan Digital Sky Survey Z' filter bandpass.

The key to minimizing the sky background and maintaining good spectrophotometric performance with the F-P etalon is for the order-sorting filters to match the free spectral range. We will operate the QI EC50WF Fabry-Perot etalon provided by Rice University at LN_2 temperatures for our near-IR work. (The etalon can also be tested at room temperature and 1 atm pressure.) The etalon coatings provide continuous wavelength coverage from 1.4 to 2.5 μm, with additional reflectivity peaks in the 0.9 to 1.33 μm range (Figure C-5). The cold cavity spacing is ~250 μm. The (laboratory) measured velocity resolution is ~26 km s^{-1} at [Fe II] 1.64μm and ~32 km s^{-1} at H_2 2.12μm. The measured finesse is ~40, with a free spectral range of 0.008 μm, or 0.4%, at 2 μm. The etalon has a 50 mm clear aperture through water-free fused silica windows. QI has indicated that only five cryogenic devices were manufactured before their engineering group disbanded, and none of the others operate at this high spectral resolution over the near-IR 0.9-2.4 μm range. The etalon will insert into the collimated beam before the stationary Lyot stop by use of a linear actuator, which minimizes the impact to the direct imaging mode. Based on our experience with other F-P systems, we do not tilt the etalon, but the science filters are tilted by 5 degrees to avoid ghosting.

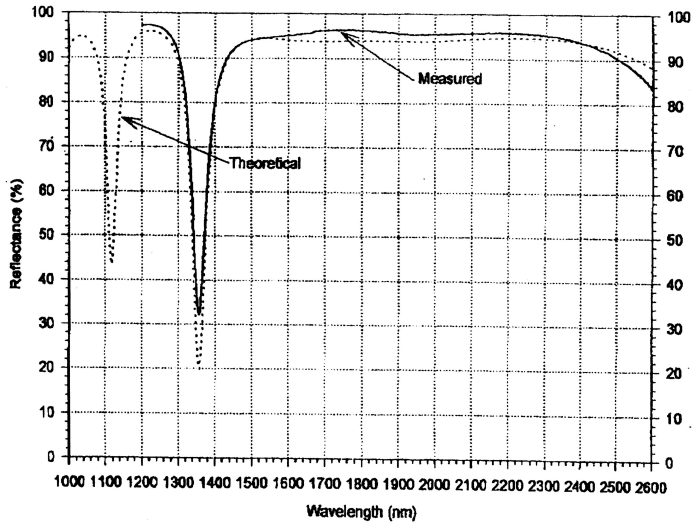

Figure C-5: *The NIC-FPS Fabry-Perot etalon reflectance measurements.*

We list our proposed set of narrow-band filters in Table C-1. These include atomic and molecular hydrogen diagnostics that cover a wide range of physical conditions that will be useful for a broad array of Galactic and extragalactic investigations. Each filter (except the Y-band filter) will have a full-width-at-half-maximum (FWHM) bandpass of 0.4% in order to match the free spectral range of the etalon. Adjacent "continuum" filters for some of the more important diagnostics will provide accurate continuum subtraction in either the F-P or direct imaging mode. These will be redshifted by one FWHM from zero-velocity to enable studies of extragalactic targets out to +1800 km s^{-1}.

The rationale for our filter selection follows. We begin with important (i.e., bright) diagnostic lines for collisionally excited gas that cover a range of temperatures: H_2 1-0 S(1) 2.12μm, ~2500K; [Fe II] 1.64μm, ~5000K; Br γ 2.16μm, ~10^4 K; and [Si VI] 1.97μm, >10^5 K. H_2 2.12μm and [Fe II] 1.64μm are probably the most commonly observed near-IR lines. We prefer Br γ to Pa β in order to avoid the forest of telluric and [Fe II] lines in close proximity to Pa β and to penetrate more obscured regions. Also, the seeing performance is somewhat better at 2.16μm than 1.28μm. [Si VI] provides a bridge between the warm ionized gas observed in H and He lines and the >10^6 K gas observed in X-rays; this line is prominent in near-IR spectra of SNRs (e.g., Gerardy & Fesen 2001) and AGN. We include redshifted/continuum filters for each of these four features. The H_2 2-1 S(1) 2.25μm line can be ratioed to H_2 1-0 S(1) 2.12μm to distinguish collisional excitation from fluorescence (Black & van Dishoeck 1987). The [Fe II] 1.26μm and 1.60μm lines can be ratioed to [Fe II] 1.64μm to measure extinction and electron density, respectively (e.g., Oliva et al. 1990). The Y-band filter (FWHM ~ 10%) will allow us to observe the [S II] 1.03μm and He I 1.08μm features using the etalon, though will transmit multiple orders; in direct imaging mode this filter can be used to search for Lyman α emission from z > 7 QSOs and is an important photometric band for studying brown dwarfs and substellar objects (Hillenbrand et al. 2002).

Figure C-6 illustrates the dramatic sky background suppression our tunable R~10,000 resolution F-P etalon will obtain compared to imagers using ~1% FWHM narrow-band filters. Instead of sky background rates of ~500-1000 photons s^{-1} $arcsec^{-2}$, we can avoid OH airglow

Table C-1. Narrow-band/Order-sorting Filter List

Species	Central Wavelength (μm)	Configuration	Notes
H_2	2.12126	v=1-0 S(1)	Shocks/Fluorescence
H_2-continuum	2.12975	v=1-0 S(1)	Redshifted
H_2	2.2471	v=2-1 S(1)	Shocks/ Fluorescence
[Fe II]	1.25668	$^6D_{9/2} - {}^4D_{7/2}$	Extinction
[Fe II]	1.59947	$^4F_{7/2} - {}^4D_{3/2}$	Electron Density
[Fe II]	1.64355	$^4F_{9/2} - {}^4D_{7/2}$	Cooling Gas
[Fe II]-continuum	1.65012	$^4F_{9/2} - {}^4D_{7/2}$	Redshifted
Br γ	2.1655	n=7 → 4	Photoionization, Shocks
Br γ-continuum	2.1742	n=7 → 4	Redshifted
[Si VI]	1.965	$^2P_{3/2} - {}^2P_{2/2}$	Hot Gas
[Si VI]-continuum	1.973	$^2P_{3/2} - {}^2P_{2/2}$	Redshifted
Y-band	1.03	–	[S II]1.03μm, He I 1.08μm, z > 7 QSOs

lines and suppress thermal continuum with the 0.01% bandpass to achieve sky rates of <10 photons s^{-1} $arcsec^{-2}$. Using this technique, a signal-to-noise ratio (S/N) calculation shows that ARC/NIC-FPS will be significantly more sensitive than Gemini/NIRI. For a uniform (monochromatic) source with an H_2 2.12μm flux of 1×10^{-17} ergs cm^{-2} s^{-1} $arcsec^{-2}$, we compute that Gemini/NIRI (8m aperture, total efficiency of 0.4, f/6 mode with 0.117 arcsec $pixel^{-1}$, H_2 filter with 1.23% FWHM, InSb detector: dark = 0.25 e^- s^{-1} $pixel^{-1}$, readnoise = 13 e^- rms $pixel^{-1}$ [16 read pairs]) achieves S/N ~ 0.6 $arcsec^{-2}$ in a 1000 sec exposure. (The on-line Gemini/NIRI integration time calculator gives S/N = 0.65.) For the same source and integration time, we calculate that ARC/NIC-FPS (3.5m aperture, total efficiency of 0.36, 0.27 arcsec $pixel^{-1}$, F-P etalon with 2.3Å bandpass at H_2, H-1RG HgCdTe detector: dark = 0.1 e^- s^{-1} $pixel^{-1}$, readnoise = 5 e^- rms $pixel^{-1}$ [16 read pairs]) will obtain S/N ~ 3 $arcsec^{-2}$.

For an F-P system, the wavelength at angle φ away from the optical axis varies as φ^2, with bluer wavelengths towards larger radii. So for extended sources (>1′), we require several exposures to cover the target. Observing in 10 velocity slices of 30 km s^{-1} each would cover a 300 kms^{-1} range over a 3.6′ diameter field. All of the tools for wavelength and flat-field calibration of F-P data, as well as correcting data cubes for off-axis wavelength dependences (phase correction), exist and will be made available for users (e.g., Bland & Tully1989; Morse et al. 1995). Figure C-7 shows an example of the deep imaging obtainable with an R~10,000 F-P system. Even at visible wavelengths, large gains can be achieved over conventional narrow-band imaging techniques. In the figure, the supernova remnant N132D is imaged in the light of [O III] 5007Å against a background of ~10^4 stars in the bar of the LMC. The very narrow bandpass of the etalon allows exquisite continuum subtraction and S/N an order of magnitude better than previous images. (Not shown is the complete velocity map that is also generated.)

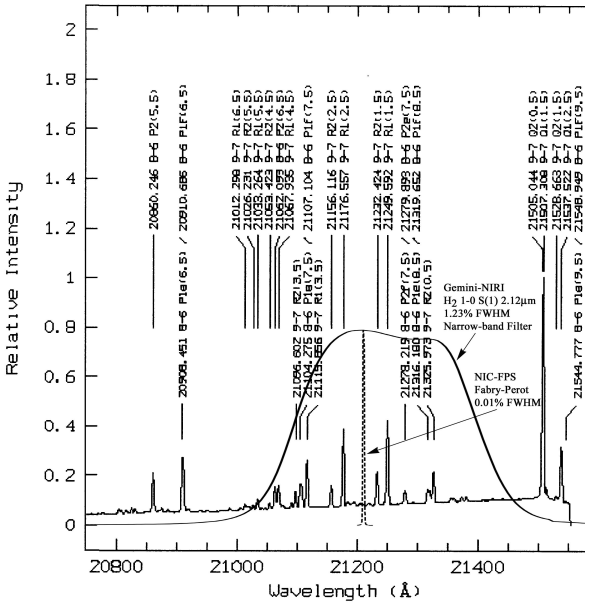

Figure C-6: *The 0.01% bandpass of the NIC-FPS Fabry-Perot etalon is compared to the 1.23% FWHM bandpass of the H_2 2.12 μm filter of the Gemini-NIRI imager. The F-P etalon will suppress the sky background by over two orders of magnitude by excluding OH airglow lines and background thermal continuum. (Sky spectrum from Lidman et al. 2000.)*

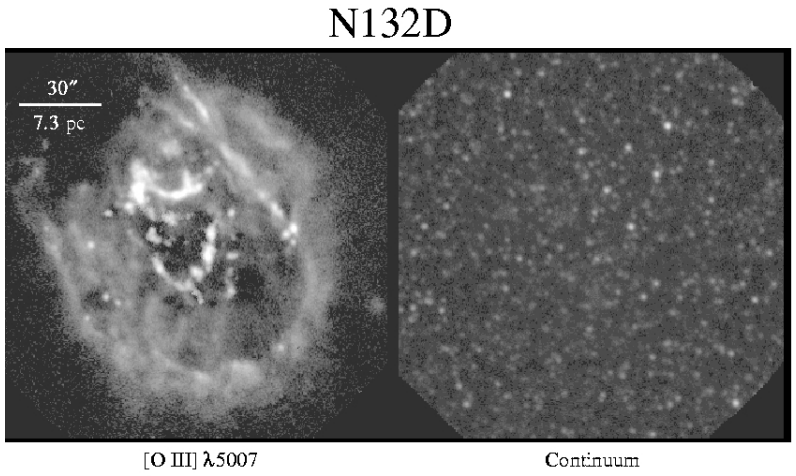

Figure C-7: *The left image shows the young SNR N132D in the bar of the LMC in the light of [O III]5007Å emission obtained with the Rutgers R~10,000 etalon on the CTIO 4-m telescope. The right image shows the off-band continuum that has been subtracted from each on-band velocity slice. The resulting continuum-subtracted images go far deeper than conventional narrow-band images. (From Morse et al. 1995.)*

Our observing plan will involve initial guaranteed runs in 2004 as detailed in the accompanying letter from APO Director, Dr. Ed Turner. We will sample representative Galactic and extragalactic targets as described herein and publicize the early results to the ARC community. Subsequent observing runs will be secured through the normal allocation process for ARC members. We are also considering future temporary deployment of NIC-FPS at the Nasmyth port of the SOAR telescope on Cerro Pachon, Chile, to enable southern sky observations and access for the broad community through the NOAO time share.

3. Instrument Description and Schedule

A description of NIC-FPS follows; a more detailed account can be found in Vincent et al. (2002). The principal members of the technical team responsible for implementing the instrument program are the present proposers (Morse, Bally, Hartigan), Mark Vincent (U. Colorado; Instrument Scientist, Optical Design), Fred Hearty (U. Colorado; Mechanical Design, Assembly, and Test), Stéphane Béland (U. Colorado; Software Development and Operations); Bruce Gillespie, Jon Holtzman, and John Barentine (Apache Point Obs.; Instrument Interfaces); and Dave Fischer, Gary Emerson, Chris Stewart, and Art Olsen (Ball Aerospace & Technologies Corp.; Systems Engineering, Opto-Mechanical Design Support).

The ARC telescope is a 3.5-m, f/10.35 modified Richey-Chretien. At 2μm, the NIC-FPS optics are designed to provide ~2 pixel sampling under good seeing conditions of ~0.5" FWHM, and 3 pixel sampling at median seeing conditions of ~0.9". These requirements lead us to select a f/3.99 camera with a 0.27" pixel^{-1} scale. The effective focal length is 13590 mm. NIC-FPS will be one of the first ground-based instruments to employ the Rockwell Hawaii-1RG 1024×1024 HgCdTe detector (1016×1016 are active), with 18 μm pixels. The field of view is 4.58' edge-to-edge, and 6.42' corner-to-corner. The geometric distortion is minimized and well characterized at 0.75% at the edges, and 1.6% at the corners. To simplify manufacturing, all surfaces on both the collimator and camera lenses are spherical. Manufacturing and alignment tolerances range from easy to moderate. The optical layout is shown in Figure C-8.

A three-element collimator will use IR-grade fused silica, CaF_2, and ZnSe elements. The first element of the collimator is located 384 mm behind the telescope focus. This distance allows the f/10.35 beam to expand to the pupil size of ~40 mm. No corrector lens is required in front of the telescope focus. The pupil is located ~301 mm behind the collimator. The space provides ample room to insert the etalon into the collimated beam. The angular magnification at the pupil is the ratio of the primary diameter to the pupil diameter, or 85×. The 0.39:1 camera has five elements composed of ZnSe, CaF_2, or fused silica. These are distributed in a triplet, followed by a singlet and a field flattener. Possible ghost images are minimized by designing a convex back surface for the corrector lens in front of the focal plane array (FPA). The optical design was initially done in Code V, and optimized in Zemax. The image quality of the baseline design is close to the diffraction limit. RMS spot diameters (that include the 3.5-m telescope performance) are maintained below the pixel size at all wavelengths and positions on the detector. The 80% diffraction encircled energy diameters are listed in Table C-2. No refocusing is necessary over the operational wavelength range.

The collimator and camera lenses will be mounted in separate aluminum optical tubes. Each tube is mounted to the cryogenic optical bench, with the contact area sized to regulate the cool-down rate. The individual lens mounts will be based on the Ohio State University Imaging Sciences Laboratory's cryogenic collet fingers design. The flexure of the collet fingers accommodates differential contraction between the lenses and the mounts without slippage. Spacing between lenses has been kept to a minimum of 5 mm to ease assembly.

NIC-FPS's exterior dimensions are 0.50 m diameter by 2.1 m long. Overall weight is estimated at 220 kg. The instrument will be mounted at a Nasmyth port on the ARC 3.5-m telescope. NIC-FPS consists of three sections: a warm cavity, the optical bench, and the LN_2 reservoir (see Figure C-9). The warm section is a 0.54 m long spacer between the telescope and the dewar, and is at ambient air pressure and temperature. The telescope focal plane is located within the warm section. Light baffling, hermetic electrical connectors and vacuum fittings are also located in the warm section. The dewar shell and optical bench are designed to ease access without disturbing the hermetic electrical connectors, LN_2 fill and vacuum fittings. When not mounted to the telescope, the instrument will be placed on a cart and rolled away from the

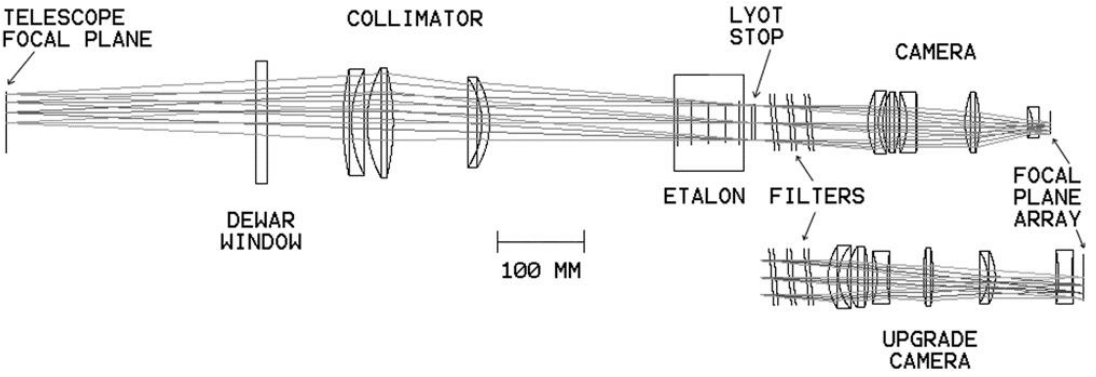

Figure C-8: *The NIC-FPS optical layout. Light is received from the 3.5-m telescope from the left. The beam enters the dewar, is collimated, passes through the etalon, cold stop, and filter wheels, then is imaged onto the detector. (The opto-mechanical layout can be upgraded to accommodate a 2k×2k detector in the future.)*

Table C-2. 80% Diffraction Encircled Energy Diameter

Wavelength (μm)	Best (μm)	Worst (μm)	Diffraction limit (μm)
0.90	11.9	17.4	11.3
1.30	16.7	20.0	16.5
2.00	27.4	37.0	25.2
2.40	32.4	39.7	30.3

* Pixel size is 18 μm. The 80% Diffraction Encircled Energy Diameter is less than 2 pixels at all locations except in the very corner of the detector at the longest wavelengths.

Nasmyth port. This cart allows removal of the dewar shell for servicing of the optical bench.

The dewar shell is a single, 1.5-m long piece extending the length of both the optical bench and the LN_2 reservoir. There is a large diameter O-ring sealed flange at each end. For maintenance of the bench, the dewar shell is broken at the front O-ring seal. The LN_2 reservoir is mounted to the back wall of the dewar shell. The shell, thermal shield and reservoir are removed as a unit. This design introduces a thermal break between the back of the optical bench and the reservoir. Copper straps and metallic springs form the thermal connection between the bench and the reservoir. The reservoir is a right circular cylinder of 30 liters volume, and has an on-axis fill/vent tube. Since NIC-FPS is mounted horizontally to a field rotator, the reservoir can only be half filled. We estimate that 15 liters of LN_2 will provide approximately 36 hour of hold time. A polished dewar interior wall and a single layer heat shield are used to reduce the radiative heat load. A Kapton sheet resistive heater attached to the LN_2 reservoir will allow a rapid, safe warm-up. Two charcoal getters will remove water from the system.

The optical bench is cantilevered from a G-10 ring, similar to Ohio State University's TIFKAM. The G-10 ring serves as both a structural support and thermal insulator. The alignment of the cantilevered bench is unaffected by the removal of the dewar shell. The optical bench serves two functions: as a mount for the optics, and a thermal conductor between the G-10 ring

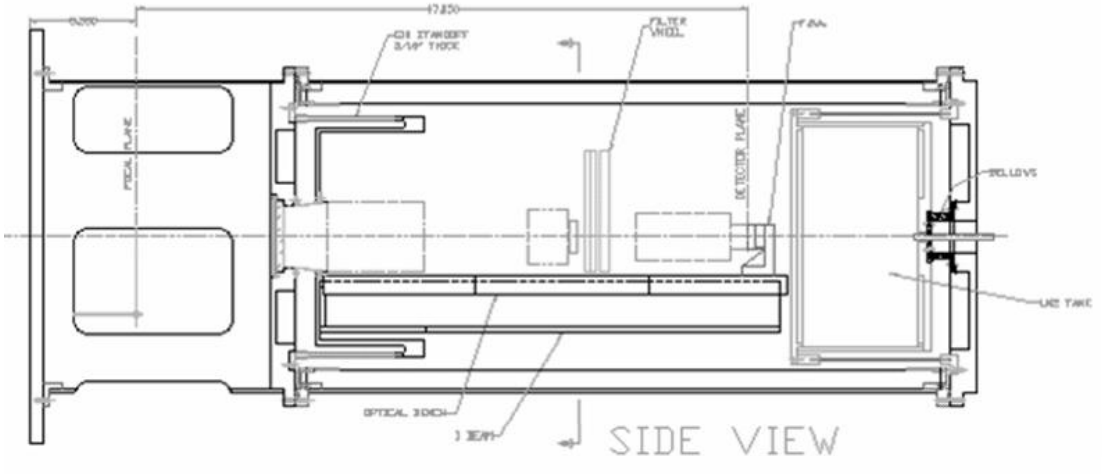

Figure C-9: *The NIC-FPS mechanical layout. Light is received from the 3.5-m telescope from the left. The dewar encloses the cantilevered optical bench (with cold optics and detector) and LN_2 reservoir.*

and LN2 reservoir. The optical bench is made rigid by two 10 cm beams, and a 2.5 cm lip around the bench's edge. The beams support the bench when it is horizontal. The bench itself resists gravitational deflection when the bench is rotated 90° to vertical on the Nasmyth port. We estimate that the bench flexure is less than 90 μm when rotating through 90°. This translates to an image shift of less than one pixel.

We will use a Rockwell Hawaii-1RG 1024×1024 pixel HgCdTe array. The pixel pitch is 18 μm. The "R" in H-1RG stands for the 4 columns of reference pixels that are located around the perimeter of the array. The reference pixels reduce the active area to 1016×1016 pixels, and will allow us to determine detector+electronics contributions to the noise in the raw images. The "G" stands for guide mode in which the electronics perform a rapid, non-destructive readout of a "postage stamp" sub-array of programmable size and location. In principle, the guide mode could be used for fast tip-tilt guiding of the ARC telescope to augment of the facility's off axis guider. The guide mode will most commonly be used to observe bright stars or planets.

The H-1RG quantum efficiency is specified to be >65% over 1-2.45 μm, though recent measurements suggest that between 75-80% is probable. The detector can be read at slow rates (100-200 kHz) to optimize readnoise performance, or at fast rates (up to 5 MHz) with selectable gain for bright scenes. Low dark current (< 0.1 $e^- s^{-1}$ $pixel^{-1}$) and readnoise (< 20 e^- rms $pixel^{-1}$ CDS) will permit long exposures of faint, extended sources observed through the etalon. The rapid read-out and deep well depth (>60,000 e^- $pixel^{-1}$) will permit observations of bright objects. We estimate 5σ detection limiting magnitudes for 1-hr (on-source) J, H, and K_s exposures of 22.5, 21.2, and 20.5, respectively. In a 1-hr integration, the 5σ limiting flux through the etalon will be ~6×10^{-18} ergs cm^{-2} s^{-1} $Å^{-1}$ $arcsec^{-2}$.

Three filter wheels with seven slots each are used to provide seventeen filter positions, one blocker (for dark frames) and three opens (one in each wheel). The wheels will be arranged in a pair and a single on opposite sides of the bench. Cryogenic stepper motors will drive the wheels through a pinion gear in contact with a spur gear located around the wheel's circumference. Roller detents in contact with the wheel's circumference will determine the final positions once the motors are turned off. An absolute position encoder will be implemented by three microswitches riding in coded grooves machined into the wheel's face. The 65 mm diameter filters will be held in cells to allow them to be removed individually using captive hardware. The general layout of the filter wheels, bearing, detents and absolute position encoders are based closely on the OSU Imaging Sciences Laboratory filter wheel design.

The NIC-FPS development schedule is shown in Figure C-10. Assembly and test of the dewar, optics, and detector system will proceed through calendar year 2003, with delivery to APO in first-quarter 2004 and commencement of science operations by mid-2004. Initiating the filter procurement using the funds from this program in ~April 2003 will allow us to receive and begin integrating the filter wheels and filters by ~September 2003. (The delivery time of the J, H, K_s filters from Barr has set our schedule.) The critical path items driving the long-term instrument development are the Hawaii-1RG detector procurement and the narrow-band filter set. We carry schedule reserve in line 44 to help offset any delivery delays.

ID	Task Name	Duration
1	**Milestones**	**657 days**
2	Project Initiation	0 days
3	Preliminary Design Review	0 days
4	Critial Design Review	1 day
5	Year 1 Review	1 day
6	Delivery to Apache Point Observatory	0 days
7	**NIC-FPS Definition**	**60 days**
8	Requirements Definition	60 days
9	**Engineering Design**	**185 days**
10	Preliminary Optical Design	65 days
11	Detailed Optical Design & Tolerances	90 days
12	Preliminary Opto-Mechanical System Design	41 days
13	Structural & Thermal Analysis	88 days
14	Detailed Dewar & Optical Bench Design	71 days
15	Filter Wheel Assembly Design	121 days
16	Lens & Filter Mount Design	121 days
17	Preliminary NIC-FPS to Telescope Interface	45 days
18	Electronics Design	120 days
19	**Procurement, Fabrication, and Assembly**	**378 days**
20	Rockwell H-1RG Eng. Array from NGST	210 days
21	Rockwell FPA Control Electronics	167 days
22	Rockwell H-1RG Science-grade Array	285 days
23	Package Engineering-grade H-1RG	45 days
24	Swap & Test Science-grade H-1RG	7 days
25	Dewar Fabrication & Assembly	120 days
26	Optical Bench Fabrication	120 days
27	Lens & Filter Mount Fabrication	90 days
28	Procure Optics	120 days
29	Filter Wheel Assembly Fab	90 days
30	Procure JHK Filters (MKO with Barr)	150 days
31	Procure Z-band Filter	150 days
32	Procure mechanism controllers	90 days
33	Procure Calibration Lamps (test use and ARC)	30 days
34	Fabricate Electronics Cabling	35 days
35	Fabricate NIC-FPS to Telescope Interface	65 days
36	**Integration, Alignment, and Test**	**288 days**
37	Lab Test Etalon and Controller Software	20 days
38	NIC-FPS Control Software Development	288 days
39	Integrate Optics into Optical Mounts	45 days
40	Integrate Optical Bench & Align Optics and Detector	90 days
41	Integrate Filter Wheels & Filters	10 days
42	Final Test & Verification	60 days
43	**Commissioning & Field Tests**	**97 days**
44	Schedule Reserve	45 days
45	Delivery to APO	0 days
46	Commissioning Run #1	5 days
47	Commissioning Run #2	5 days
48	Begin Science Operations	1 day

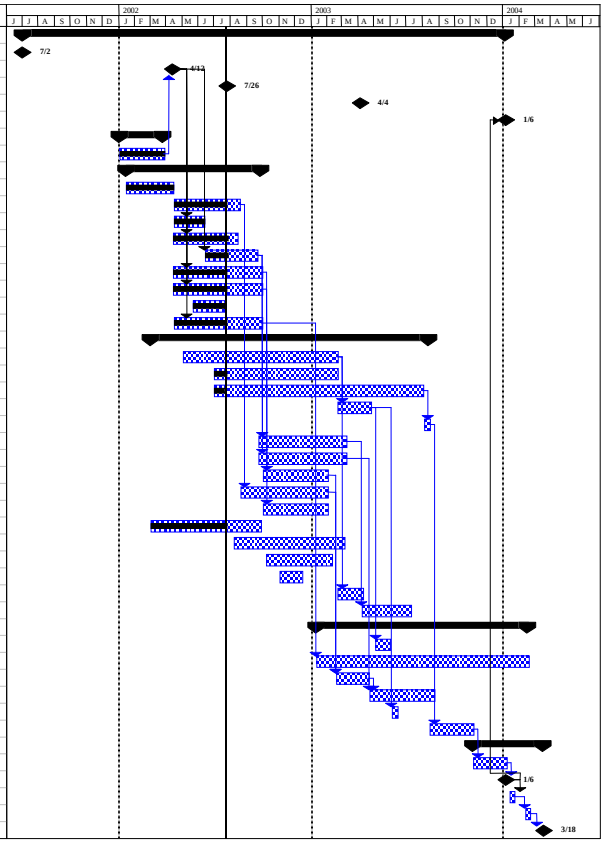

Figure C-10: *The NIC-FPS development schedule (as of July CDR).*

As noted in Section 1, the NIC-FPS development is a ~$1.1M joint internal effort against which we are leveraging the request for funds in this proposal. The hardware comprises ~$600K (not including the narrow-band filter set), the largest expenditures being the Rockwell Hawaii-1RG detector and control electronics package (~$300K) and the cryogenic F-P etalon ($62K purchase price). Funding for a new CS-100 etalon controller is also part of our current request.

4. Teaching, Student Participation, and Outreach

NIC-FPS development is shared primarily among rostered faculty, research associates, and graduate students at CU-CASA. As with CASA's UV sounding rocket program, a graduate student (Mr. Fred Hearty) assumes major responsibilities for the opto-mechanical implementation as part of his training in precision astronomical instrumentation. CU-CASA holds a firm commitment to the training of the next generation of instrumentalists and observational astronomers through student participation in hardware development and observing programs using ground- and space-based facilities. One of the reasons CU joined ARC in 2001 was the close proximity of APO, which facilitates student participation in collaborative research programs. After NIC-FPS is commissioned, students will have access to the instrument through CU's share of telescope time. Results from NIC-FPS will be integrated into CU's (and Rice's) teaching curriculum for majors and non-majors, just as our *HST* and *FUSE* programs have been in the past. Results will also be incorporated into faculty-designed educational shows at CU's Fiske Planetarium which hosts regular K-12 and public outreach events throughout the year.